

MATRO: Metric-Aware Trust-Region Optimization with Fully Quadratic Models

Wei Hu* Pengcheng Xie† Ya-Xiang Yuan‡ Li Zhang§

June 2, 2026

Abstract

Model-based derivative-free trust-region methods build local interpolation models and restrict trial steps to regions where those models are reliable. This paper studies the shape of that region. When an objective is poorly scaled or locally anisotropic, a Euclidean ball can be governed by the steepest local direction and can restrict progress along directions of slow variation. We propose MATRO (Metric-Aware Trust-Region Optimization), a fully quadratic interpolation framework in which the trust region is the ellipsoid $s^\top M_k s \leq \Delta_k^2$. For any positive definite metric M_k , the induced variable $y = M_k^{1/2} s$ converts the ellipsoidal subproblem into a standard Euclidean trust-region subproblem, so model decrease, ratio tests, radius updates, poisedness, and fully quadratic error bounds can be stated in induced coordinates under a uniform metric contract. The metric is selected from the interpolation Hessian: positive definite quadratics yield a unique volume-normalized curvature metric that isotropizes the induced Hessian and gives a truncated Newton step, while indefinite fitted Hessians motivate an absolute-curvature metric that balances curvature magnitudes without changing curvature signs. Under the standard fully quadratic assumptions and the metric contract, MATRO retains the first-order evaluation-complexity order $\mathcal{O}(n^2 \varepsilon^{-2})$. Experiments on Moré–Wild benchmarks, controlled anisotropy tests, and two-dimensional trajectories show that curvature-shaped regions are most effective when the interpolation Hessian captures stable local anisotropy, while dense linear algebra is most visible at loose accuracies or on inexpensive analytic tests.

Keywords. derivative-free optimization, trust-region methods, fully quadratic models, ellipsoidal trust regions, metric selection, evaluation complexity

AMS subject classifications. 65K05, 90C56, 90C30

1 Introduction

Derivative-free optimization (DFO) addresses problems in which function values are available but reliable derivatives are not. Such problems arise when the objective is produced by a simulation, experiment, or legacy code, and a single evaluation may be far more expensive than the algebra performed by the optimizer. Model-based trust-region methods form one of the main deterministic approaches in this setting: they construct a local surrogate from sampled

*LSEC, ICMSEC, Academy of Mathematics and Systems Science, Chinese Academy of Sciences, Beijing 100190, China; and University of Chinese Academy of Sciences, Beijing 100049, China (huwei@amss.ac.cn). Corresponding author.

†Lawrence Berkeley National Laboratory, Berkeley, CA 94720, USA (pxie98@gmail.com).

‡LSEC, ICMSEC, Academy of Mathematics and Systems Science, Chinese Academy of Sciences, Beijing 100190, China (yyx@lsec.cc.ac.cn).

§LSEC, ICMSEC, Academy of Mathematics and Systems Science, Chinese Academy of Sciences, Beijing 100190, China (zhangli2022@lsec.cc.ac.cn).

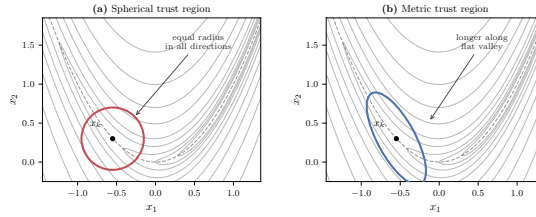


Figure 1: Spherical and metric trust regions on Rosenbrock-type contours. A ball in the original variables uses the same length scale in every direction, whereas an ellipsoid can be aligned with a local valley. The figure is illustrative: MATRO constructs the metric from interpolation curvature, not from exact derivative information.

values, minimize the surrogate in a neighborhood of the current point, and accept the trial point according to the agreement between actual and predicted reduction [5, 8].

The standard analysis of interpolation-based DFO is built around two ingredients: a local model that is accurate enough near the current point and a sampling set with adequate geometry. Fully linear and fully quadratic models, together with poised interpolation sets, make this principle precise. The present paper studies a related geometric choice that is often fixed before the analysis begins: the shape of the region where the model is trusted. Most interpolation-based trust-region solvers use a Euclidean ball in the original variables. This convention is stable and simple to manage, but it represents all directions by a single scalar radius.

A single scalar radius can be restrictive in poorly scaled or locally anisotropic regions. A narrow curved valley gives the basic example. Across the valley the objective changes rapidly, so a reliable model may require short transverse steps. Along the valley floor the objective changes more slowly, and longer steps may be beneficial. A spherical trust region must compromise between these two scales. If the radius is chosen for the transverse direction, movement along the valley floor may be needlessly slow; if it is chosen for the tangential direction, the trial step may leave the region in which the model is reliable across the valley. This is not simply a failure of variable preprocessing. The relevant directions can rotate during the run, and in a black-box setting they must be inferred from the function values already collected.

Changing the shape of the trust region is equivalent to changing the metric in the trust-region subproblem. For a symmetric positive definite matrix M_k , define

$$\mathcal{B}_{M_k}(x_k, \Delta_k) := \{x_k + s : s^\top M_k s \leq \Delta_k^2\}. \quad (1)$$

The scalar Δ_k controls the size of the region, while M_k controls its shape and orientation. With the induced variable

$$y = M_k^{1/2} s, \quad (2)$$

the ellipsoid (1) becomes the Euclidean ball $\|y\| \leq \Delta_k$. Thus an ellipsoidal subproblem in the original variables is an ordinary Euclidean trust-region subproblem after a linear change of coordinates. This simple observation is the first organizing principle of the paper: the trust-region mechanism can be analyzed for an arbitrary bounded metric before any particular metric-selection rule is specified.

The second organizing principle is that a fully quadratic DFO method already computes a Hessian matrix. Classical full quadratic solvers use this matrix in the quadratic objective but usually leave the trusted region spherical in the original variables. We ask whether the same fitted curvature can also define the shape of the region over which the model is trusted. This question is meaningful only if the metric is stable: the fitted Hessian may be inaccurate in early iterations, nearly singular, or indefinite. The role of the metric is therefore not to convexify the model. The signed Hessian remains in the trust-region subproblem, and the metric supplies a positive definite length scale for the step.

Table 1: The quadratic model $f(x) = \frac{1}{2}x^\top \text{diag}(1, \kappa)x$. The induced condition number is that of $M^{-1/2}HM^{-1/2}$.

Metric M	Induced condition number	Semi-axis lengths
I	κ	Δ, Δ
$\text{diag}(\kappa^{-1/2}, \kappa^{1/2})$	1	$\Delta\kappa^{1/4}, \Delta\kappa^{-1/4}$
$\text{diag}(K^{-1/2}, K^{1/2}), K \leq \kappa$	κ/K	$\Delta K^{1/4}, \Delta K^{-1/4}$

The ideal positive definite case explains the construction. For the quadratic

$$f(x) = \frac{1}{2}x^\top Hx, \quad H = \text{diag}(1, \kappa), \quad \kappa \gg 1, \quad (3)$$

the Euclidean metric leaves the induced Hessian with condition number κ . The volume-normalized curvature metric

$$M_\star = \frac{H}{\det(H)^{1/2}} = \text{diag}(\kappa^{-1/2}, \kappa^{1/2}) \quad (4)$$

gives

$$M_\star^{-1/2}HM_\star^{-1/2} = \kappa^{1/2}I. \quad (5)$$

Thus the quadratic is isotropic in the variables used by the subproblem. In the original variables, the trust region expands along the flat direction and contracts along the steep direction. If a condition-number cap $\text{cond}(M) \leq K$ is imposed for stability, the best commuting metric in this two-dimensional example can remove only a factor K of the original condition number. Table 1 summarizes this calculation.

The paper develops MATRO (Metric-Aware Trust-Region Optimization) around these ideas. The first part establishes the metric trust-region framework: metric balls, induced-coordinate subproblems, poisedness in metric balls, and a metric contract that keeps the analysis uniform. The second part constructs metrics from interpolation curvature. For positive definite quadratics, the determinant-normalized Hessian is the unique volume-normalized metric that makes the induced Hessian isotropic; moreover, the corresponding metric trust-region step is a truncated Newton step. For indefinite Hessians, an absolute-curvature metric balances curvature magnitudes while preserving the signs of the model curvature. Stabilized spectral variants satisfy the metric contract needed for the standard fully quadratic convergence proof. The numerical experiments then examine the expected cost–accuracy trade-off: curvature-shaped regions can help when the fitted Hessian captures persistent anisotropy, but they require full quadratic models and dense linear algebra.

1.1 Related work

The algorithmic setting is the model-based DFO trust-region framework. The monograph of Conn, Scheinberg, and Vicente [5] develops fully linear and fully quadratic model theory, criticality steps, geometry-improvement mechanisms, and evaluation-complexity analysis for interpolation-based DFO. The classical derivative-based trust-region background is given by Conn, Gould, and Toint [2], and the geometry of interpolation and regression sets is analyzed in [3, 4]. Powell’s solvers are central practical references: UOBYQA uses full quadratic interpolation [11], whereas NEWUOA and BOBYQA reduce the number of points through minimum-change Hessian updates [12, 13]. PRIMA provides a modern reference implementation of Powell’s methods [23].

A recent line of work has emphasized that the model-construction rule itself is a mathematical design choice. Examples include underdetermined models derived from trust-region iteration properties [15, 17–19], least H^2 -norm updating [16], regional minimal updating [20], transformed-objective DFO [21], and two-dimensional model-based subspace methods [22]. These works

modify the norm, update criterion, transformation, or subspace used to construct a local model. MATRO is complementary to this direction. It keeps the model fully quadratic and treats a different object as design variable: the metric defining where the model is trusted.

Scaling and preconditioning are classical in smooth trust-region methods [2]. Their derivative-free use is subtler because the relevant local geometry is not normally available from exact derivatives. A fixed change of variables can remove known parameter scales, but it does not generally follow a local curvature geometry that rotates or changes during the run. Other DFO algorithms adapt geometry in different ways: MADS adapts polling directions in a direct-search framework [1], RBF trust-region methods build nonpolynomial local surrogates [14], and CMA-ES adapts a covariance matrix in a population-based stochastic search [7]. The present work remains within deterministic interpolation-based trust regions and asks how the curvature already present in a fully quadratic model can be converted into a stable ellipsoidal trust-region shape. Three features distinguish MATRO from Hessian-scaled trust regions in the smooth setting: (i) the metric is derived from an *interpolation* Hessian that may be inaccurate or indefinite, not from an exact gradient or Hessian; (ii) the metric defines only the trust-region geometry, while the signed Hessian is retained in the subproblem objective—the model is not convexified; and (iii) the metric changes at every iteration and must satisfy a uniform spectral contract to preserve the fully quadratic convergence machinery.

1.2 Notation

Throughout the paper, \mathbb{R}^n is equipped with the standard inner product $\langle u, v \rangle = u^\top v$ and Euclidean norm $\|u\|$. For $M \succ 0$, define $\|u\|_M = (u^\top M u)^{1/2}$, and let $M^{1/2}$ denote the SPD square root. For a symmetric matrix H , define

$$\|H\|_M := \left\| M^{-1/2} H M^{-1/2} \right\|_2. \quad (6)$$

If $H \succ 0$, write

$$\kappa_M(H) := \text{cond}(M^{-1/2} H M^{-1/2}). \quad (7)$$

The condition number is $\text{cond}(M) = \lambda_{\max}(M)/\lambda_{\min}(M)$, and $A \preceq B$ means that $B - A$ is positive semidefinite. At iteration k , x_k is the current point, Δ_k is the trust-region radius, M_k is the metric, and $T_k = M_k^{1/2}$. In induced coordinates $y = T_k s$, the model gradient and Hessian are denoted by $g_{y,k}$ and $B_{y,k}$. We use

$$\chi_k = \|g_{y,k}\|, \quad \chi_k^{\text{true}} = \left\| M_k^{-1/2} \nabla f(x_k) \right\| \quad (8)$$

for the model and true metric-dual stationarity measures.

2 Metric Trust-Region Framework

The metric will later be selected from interpolation curvature, but the basic trust-region mechanism does not depend on that choice. This section fixes an arbitrary positive definite metric and rewrites the usual trust-region ingredients in the induced coordinates where the metric ball is Euclidean. The identities below are elementary, but they are the mechanism that allows the later analysis to separate trust-region globalization from metric selection.

2.1 Metric balls and volume

Given $x \in \mathbb{R}^n$, $\Delta > 0$, and $M \succ 0$, define the metric ball

$$\mathcal{B}_M(x, \Delta) := \{x + s : \|s\|_M \leq \Delta\}. \quad (9)$$

If $M = Q \operatorname{diag}(\mu_1, \dots, \mu_n) Q^\top$, with Q orthogonal and $\mu_i > 0$, then $\mathcal{B}_M(x, \Delta)$ is an ellipsoid with principal directions given by the columns of Q and semi-axis lengths $\Delta/\sqrt{\mu_i}$. Its volume is

$$\operatorname{vol}(\mathcal{B}_M(x, \Delta)) = \omega_n \Delta^n \det(M)^{-1/2}, \quad (10)$$

where ω_n is the volume of the Euclidean unit ball in \mathbb{R}^n .

Proposition 2.1 (Axes and volume of a metric ball). *Let $M \succ 0$ have the spectral decomposition $M = Q \operatorname{diag}(\mu_1, \dots, \mu_n) Q^\top$. Then $\mathcal{B}_M(x, \Delta)$ has semi-axis lengths $\Delta/\sqrt{\mu_i}$ along Qe_i , and its volume is given by (10). If $\det(M) = 1$, then $\mathcal{B}_M(x, \Delta)$ and $B(x, \Delta)$ have the same volume; the matrix M changes the shape but not the volume scale.*

Proof. Write $s = Qz$. Then $s^\top Ms = \sum_i \mu_i z_i^2$. The boundary condition $s^\top Ms = \Delta^2$ gives the semi-axis lengths $\Delta/\sqrt{\mu_i}$. The change of variables $y = M^{1/2}s$ maps the ellipsoid onto the Euclidean ball $\|y\| \leq \Delta$ and has Jacobian determinant $\det(M)^{1/2}$. Hence $\operatorname{vol}(\mathcal{B}_M) = \det(M)^{-1/2} \omega_n \Delta^n$. \square

Theorem 2.1 explains the determinant normalization used in Section 3. The trust-region radius already controls the overall size of the trusted region. The metric is used to distribute this size among directions. Setting $\det(M) = 1$ is a convenient way to keep this separation explicit.

2.2 Subproblems in induced variables

Let $M \succ 0$, $T = M^{1/2}$, and $y = Ts$. The model in the original step variable is

$$m_x(s) = f(x) + g_x^\top s + \frac{1}{2} s^\top H_x s. \quad (11)$$

Define the induced model \tilde{m} by

$$\tilde{m}(y) = m_x(T^{-1}y). \quad (12)$$

Theorem 2.2 (Equivalence of metric and Euclidean subproblems). *Let $M \succ 0$, $T = M^{1/2}$, and $y = Ts$. The two optimization problems*

$$\min_{\|s\|_M \leq \Delta} m_x(s), \quad \min_{\|y\| \leq \Delta} \tilde{m}(y) \quad (13)$$

are equivalent under the change of variables $y = Ts$ and have the same optimal value. Moreover, predicted reduction is preserved:

$$m_x(0) - m_x(s) = \tilde{m}(0) - \tilde{m}(y), \quad y = Ts, \quad (14)$$

and the gradient and Hessian in induced variables are

$$g_y = T^{-1}g_x, \quad B_y = T^{-1}H_x T^{-1}. \quad (15)$$

Proof. Since T is SPD, $\|s\|_M^2 = s^\top T^2 s = \|Ts\|^2 = \|y\|^2$. Hence feasibility is preserved by $y = Ts$. Substitution gives

$$m_x(T^{-1}y) = f(x) + g_x^\top T^{-1}y + \frac{1}{2} y^\top T^{-1}H_x T^{-1}y. \quad (16)$$

The equality of optimal values and predicted reductions follows immediately, and the expressions in (15) follow by differentiation. \square

The standard Cauchy decrease condition can also be written directly in the metric of the original variables. This form makes clear how the choice of M enters the first-order decrease mechanism. For a symmetric matrix H , write

$$\|H\|_M := \left\| M^{-1/2} H M^{-1/2} \right\|_2.$$

Proposition 2.3 (Metric form of Cauchy decrease). *Let m_x be given by (11). Suppose that the induced step y satisfies the usual Cauchy decrease condition for \tilde{m} on $\|y\| \leq \Delta$:*

$$\tilde{m}(0) - \tilde{m}(y) \geq \frac{1}{2} \|g_y\| \min \left\{ \Delta, \frac{\|g_y\|}{\|B_y\|_2} \right\}, \quad (17)$$

with the convention that the quotient is $+\infty$ when $B_y = 0$. Then $s = T^{-1}y$ satisfies

$$m_x(0) - m_x(s) \geq \frac{1}{2} \|g_x\|_{M^{-1}} \min \left\{ \Delta, \frac{\|g_x\|_{M^{-1}}}{\|H_x\|_M} \right\}. \quad (18)$$

Proof. By (15),

$$\|g_y\| = \|M^{-1/2}g_x\| = \|g_x\|_{M^{-1}}, \quad \|B_y\|_2 = \|M^{-1/2}H_xM^{-1/2}\|_2 = \|H_x\|_M.$$

The predicted reduction identity (14) then turns (17) into (18). \square

2.3 Poisedness in metric balls

At iteration k , the modeled function in induced variables is

$$\tilde{f}_k(y) = f(x_k + T_k^{-1}y), \quad \|y\| \leq \Delta_k, \quad (19)$$

where $T_k = M_k^{1/2}$. Let

$$q_n = \frac{(n+1)(n+2)}{2} \quad (20)$$

be the dimension of the quadratic polynomial space. A full quadratic interpolation model in induced variables has the form

$$\tilde{m}_k(y) = f(x_k) + g_{y,k}^\top y + \frac{1}{2} y^\top B_{y,k} y. \quad (21)$$

The trial step is computed from

$$\min_{\|y\| \leq \Delta_k} g_{y,k}^\top y + \frac{1}{2} y^\top B_{y,k} y, \quad (22)$$

and the original step is $s_k = T_k^{-1}y_k$. If the model is expressed in the original variables, its Hessian is

$$H_{x,k} = T_k B_{y,k} T_k. \quad (23)$$

This matrix is the curvature information passed to the metric-selection routine.

We use the standard notion of Λ -poisedness in Euclidean coordinates, but apply it after the induced-coordinate map. This convention matters because changing M_k changes the coordinates in which archived points are viewed.

Definition 2.4 (Poisedness in a metric ball). Let $M \succ 0$, $T = M^{1/2}$, and let $Y = \{x + s^{(0)}, \dots, x + s^{(q_n-1)}\} \subset \mathcal{B}_M(x, \Delta)$. We say that Y is Λ -poised in $\mathcal{B}_M(x, \Delta)$ if the transformed set

$$\tilde{Y} = \{Ts^{(0)}, \dots, Ts^{(q_n-1)}\} \quad (24)$$

is Λ -poised in the Euclidean ball $B(0, \Delta)$ for quadratic interpolation.

Metric poisedness is the usual poisedness condition applied in the variables in which the trust region is a ball. The classical fully quadratic interpolation theory can therefore be used once all quantities are written in induced coordinates.

Algorithm 1 Abstract MATRO method

Require: Objective f , initial point x_0 , radius $\Delta_0 > 0$, parameters $0 < \eta_1 \leq \eta_2 < 1$, $0 < \gamma_{\text{dec}} < 1 < \gamma_{\text{inc}}$, criticality constant μ_{crit} , and a METRICSELECTION routine. The criticality threshold is normalized to one.

- 1: Set $M_0 = I$, $T_0 = I$, and initialize the archive with $(x_0, f(x_0))$.
- 2: Build an initial Λ -poised set of q_n points in induced coordinates; evaluate f and add the points to the archive.
- 3: **for** $k = 0, 1, 2, \dots$ **do**
- 4: **repeat**
- 5: Select or repair a Λ -poised interpolation set in $\|y\| \leq \Delta_k$; fit \tilde{m}_k in (21).
- 6: **if** $\|g_{y,k}\| \leq 1$ and $\Delta_k > \mu_{\text{crit}} \|g_{y,k}\|$ **then**
- 7: Set $\Delta_k \leftarrow \mu_{\text{crit}} \|g_{y,k}\|$.
- 8: **end if**
- 9: **until** $\|g_{y,k}\| > 1$ or $\Delta_k \leq \mu_{\text{crit}} \|g_{y,k}\|$
- 10: Approximately solve (22) to obtain y_k satisfying the Cauchy decrease condition.
- 11: Set $s_k = T_k^{-1} y_k$; evaluate $f(x_k + s_k)$ and add the trial point to the archive.
- 12: Compute $\text{pred}_k = \tilde{m}_k(0) - \tilde{m}_k(y_k)$ and $\text{ared}_k = f(x_k) - f(x_k + s_k)$.
- 13: Set $\rho_k = \text{ared}_k / \text{pred}_k$ if $\text{pred}_k > 0$, and $\rho_k = -\infty$ otherwise.
- 14: Accept $x_{k+1} = x_k + s_k$ if $\rho_k \geq \eta_1$; otherwise set $x_{k+1} = x_k$.
- 15: Update Δ_{k+1} by the standard trust-region rule.
- 16: Form $H_{x,k} = T_k B_{y,k} T_k$, set $M_{k+1} = \text{METRICSELECTION}(H_{x,k}, M_k, A_k, \Delta_k; \theta)$, and set $T_{k+1} = M_{k+1}^{1/2}$.
- 17: **end for**

2.4 The abstract algorithm

The metric update is written abstractly as

$$M_{k+1} = \text{METRICSELECTION}(H_{x,k}, M_k, A_k, \Delta_k; \theta), \quad (25)$$

where A_k is the archive of sampled points and θ denotes fixed metric parameters. The convergence proof uses only the following contract.

Assumption 2.5 (Uniform metric bounds). *There exist constants $0 < m_{\min} \leq m_{\max} < \infty$ such that every metric returned by METRICSELECTION satisfies*

$$m_{\min} I \preceq M_k \preceq m_{\max} I, \quad k = 0, 1, 2, \dots \quad (26)$$

Algorithm 1 is the abstract method analyzed in Section 4. The specific spectral rule used in the experiments is introduced in Section 3. Implementation safeguards used in the numerical section, such as a lower radius bound or adaptive initialization, are not part of the complexity proof.

3 Metrics from Interpolation Curvature

We now turn from the abstract metric framework to the construction of the metric. The guiding object is the Hessian of the fully quadratic interpolation model. When the interpolation geometry is adequate and the radius is small, this Hessian approximates the true local Hessian; before that asymptotic regime is reached, it remains the only second-order object available to a fully quadratic DFO method. The analysis in this section explains how much one can gain from this curvature, what is lost when the metric must be capped for stability, and how the same idea should be interpreted when the fitted Hessian is indefinite.

3.1 Induced conditioning as a metric criterion

For an SPD curvature matrix H , a natural measure of the anisotropy left after choosing $M \succ 0$ is

$$\kappa_M(H) = \text{cond}(M^{-1/2}HM^{-1/2}). \quad (27)$$

This quantity is the condition number of the quadratic model in induced variables. Since multiplying M by a positive scalar can be absorbed into the radius, we fix the scale by imposing $\det(M) = 1$. The idealized design problem for a positive definite quadratic model is therefore

$$\text{choose } M \succ 0, \quad \det(M) = 1, \quad \text{so that } \text{cond}(M^{-1/2}HM^{-1/2}) \text{ is small.} \quad (28)$$

The next results follow this design problem from the ideal SPD case to the stabilized rule used by the algorithm. The order is deliberate: first the exact quadratic calculation identifies the metric one would choose if the curvature were known and positive definite; then the cap, approximation error, and indefinite-curvature cases explain the modifications needed in a derivative-free implementation.

3.2 Positive curvature and Newton rays

The exact SPD quadratic case provides the reference point for the whole construction. Here the curvature matrix is both a reliable local model Hessian and a valid positive definite shape matrix. The determinant constraint removes irrelevant scaling and leaves a pure shape-selection problem.

Proposition 3.1 (Optimal metric for positive definite quadratics). *Let $H \succ 0$ and define*

$$\mathcal{M}_{\det} := \{M \succ 0 : \det(M) = 1\}. \quad (29)$$

Then

$$M_{\star} = \frac{H}{\det(H)^{1/n}} \quad (30)$$

belongs to \mathcal{M}_{\det} and satisfies

$$M_{\star}^{-1/2}HM_{\star}^{-1/2} = \det(H)^{1/n}I. \quad (31)$$

Consequently, $\kappa_{M_{\star}}(H) = 1$, which is the minimum possible induced condition number. The minimizer is unique under the determinant constraint.

Proof. Let $\alpha = \det(H)^{1/n}$. Then $M_{\star} = H/\alpha$ and $\det(M_{\star}) = \det(H)/\alpha^n = 1$. Moreover $M_{\star}^{-1/2} = \alpha^{1/2}H^{-1/2}$, so $M_{\star}^{-1/2}HM_{\star}^{-1/2} = \alpha I$. No SPD matrix can produce an induced condition number below one. If another $M \in \mathcal{M}_{\det}$ also gives condition number one, then $M^{-1/2}HM^{-1/2} = \beta I$ for some $\beta > 0$, hence $H = \beta M$. Taking determinants gives $\det(H) = \beta^n \det(M) = \beta^n$, so $\beta = \det(H)^{1/n}$ and $M = H/\beta = M_{\star}$. \square

The preceding proposition describes the shape of the quadratic in induced variables. The next proposition translates that shape statement into the actual step. With the curvature metric, the constrained step follows the Newton ray and is shortened only when the metric radius cuts off the full Newton step.

Proposition 3.2 (Newton-ray property of the curvature metric). *Let*

$$m(s) = f_0 + g^{\top}s + \frac{1}{2}s^{\top}Hs, \quad H \succ 0, \quad (32)$$

and let $M = H/\alpha$, where $\alpha = \det(H)^{1/n}$. The solution of

$$\min_{s^\top Ms \leq \Delta^2} g^\top s + \frac{1}{2} s^\top H s \quad (33)$$

is

$$s_\Delta = -t_\Delta H^{-1}g, \quad t_\Delta = \min \left\{ 1, \Delta \sqrt{\frac{\alpha}{g^\top H^{-1}g}} \right\}, \quad (34)$$

with the convention that $s_\Delta = 0$ if $g = 0$. Moreover,

$$m(0) - m(s_\Delta) = t_\Delta \left(1 - \frac{t_\Delta}{2} \right) g^\top H^{-1}g. \quad (35)$$

Proof. If $g = 0$, the claim is immediate. Assume $g \neq 0$. In the induced variables $y = M^{1/2}s$, the Hessian is $M^{-1/2}HM^{-1/2} = \alpha I$ by Theorem 3.1, and the gradient is $g_y = M^{-1/2}g = \alpha^{1/2}H^{-1/2}g$. Hence the induced subproblem is

$$\min_{\|y\| \leq \Delta} g_y^\top y + \frac{\alpha}{2} \|y\|^2. \quad (36)$$

Its unconstrained minimizer is $-\alpha^{-1}g_y$, whose norm is $\sqrt{g^\top H^{-1}g/\alpha}$. If this point is feasible, then $t_\Delta = 1$. Otherwise the minimizer is the boundary point in the direction $-g_y$, which corresponds to $t_\Delta = \Delta \sqrt{\alpha/(g^\top H^{-1}g)}$. Mapping back by $s = M^{-1/2}y$ gives (34). Substitution into (32) gives (35). \square

Corollary 3.3 (One-step recovery for exact positive definite quadratics). *Let $f(x) = f_\star + \frac{1}{2}(x - x_\star)^\top H(x - x_\star)$ with $H \succ 0$. Suppose that the interpolation model is exact at x_k , and let $g_k = \nabla f(x_k)$ and $M_k = H/\det(H)^{1/n}$. If*

$$\Delta_k \geq \sqrt{\frac{g_k^\top H^{-1}g_k}{\det(H)^{1/n}}}, \quad (37)$$

then the metric trust-region step gives $x_{k+1} = x_\star$. If (37) fails, the step lies on the Newton ray $x_k - tH^{-1}g_k$ with $0 < t < 1$.

Proof. Apply Theorem 3.2 with $g = g_k$. The unconstrained Newton step $-H^{-1}g_k$ reaches x_\star . The feasibility condition is exactly (37). \square

The same calculation also gives the Cauchy decrease constant used below. For $M = H/\alpha$, $\|H\|_M = \alpha$ and $\|g\|_{M^{-1}}^2 = \alpha g^\top H^{-1}g$. Thus the metric Cauchy decrease in Theorem 2.3 is expressed through the Newton decrement $g^\top H^{-1}g$ and the geometric-mean curvature α , instead of through the largest eigenvalue of H . This is one way in which the metric changes constants without changing the standard trust-region order of complexity.

3.3 The effect of a metric cap

In practice, a metric with a very large condition number is undesirable. It can make archived interpolation points poorly distributed in induced coordinates and can amplify roundoff errors. A condition-number cap restricts the amount of anisotropy allowed in the trust region. The next result shows that such a cap also imposes a fundamental limit: no metric with $\text{cond}(M) \leq K$ can remove more than a factor K of the condition number of an SPD quadratic.

Proposition 3.4 (Conditioning limit under a metric cap). *Let $H \succ 0$ and let $M \succ 0$ satisfy $\text{cond}(M) \leq K$. Then*

$$\text{cond}(M^{-1/2}HM^{-1/2}) \geq \frac{\text{cond}(H)}{K}. \quad (38)$$

Proof. Using the generalized Rayleigh quotient,

$$\lambda_{\max}(M^{-1/2}HM^{-1/2}) = \max_{v \neq 0} \frac{v^\top H v}{v^\top M v} \geq \frac{\lambda_{\max}(H)}{\lambda_{\max}(M)}, \quad (39)$$

and

$$\lambda_{\min}(M^{-1/2}HM^{-1/2}) = \min_{v \neq 0} \frac{v^\top H v}{v^\top M v} \leq \frac{\lambda_{\min}(H)}{\lambda_{\min}(M)}. \quad (40)$$

Taking the ratio gives

$$\text{cond}(M^{-1/2}HM^{-1/2}) \geq \frac{\lambda_{\max}(H)}{\lambda_{\min}(H)} \frac{\lambda_{\min}(M)}{\lambda_{\max}(M)} = \frac{\text{cond}(H)}{\text{cond}(M)} \geq \frac{\text{cond}(H)}{K}. \quad (41)$$

□

For the two-dimensional quadratic in Table 1, the bound is attained by the capped metric $M_K = \text{diag}(K^{-1/2}, K^{1/2})$. Thus the cap is not only a numerical safeguard; it also quantifies the maximum conditioning improvement that the chosen metric class can express.

3.4 Metric accuracy from interpolation curvature

The interpolation Hessian is only an approximation. We first record a perturbation statement: if a metric is close to a curvature shape in Loewner order, then the induced Hessian is well conditioned.

Proposition 3.5 (Induced conditioning from Loewner alignment). *Let $M \succ 0$ and $H_{\text{shape}} \succ 0$. Suppose there exist $\alpha > 0$ and $\delta \geq 0$ such that*

$$e^{-\delta}\alpha M \preceq H_{\text{shape}} \preceq e^{\delta}\alpha M. \quad (42)$$

Then

$$\text{cond}(M^{-1/2}H_{\text{shape}}M^{-1/2}) \leq e^{2\delta}. \quad (43)$$

Proof. Premultiplying and postmultiplying (42) by $M^{-1/2}$ gives

$$e^{-\delta}\alpha I \preceq M^{-1/2}H_{\text{shape}}M^{-1/2} \preceq e^{\delta}\alpha I. \quad (44)$$

All eigenvalues of the induced matrix lie in $[e^{-\delta}\alpha, e^{\delta}\alpha]$, and their ratio is at most $e^{2\delta}$. □

For a fully quadratic model, this alignment estimate can be read directly from the Hessian error bound.

Corollary 3.6 (Fully quadratic Hessian error and metric accuracy). *Let $H_\star \succ 0$ with $\lambda_{\min}(H_\star) \geq \nu > 0$, and let $H \succ 0$ satisfy*

$$\|H - H_\star\|_2 \leq \kappa_H \Delta, \quad \theta := \frac{\kappa_H \Delta}{\nu} < 1. \quad (45)$$

Let $M = H / \det(H)^{1/n}$. Then

$$\text{cond}(M^{-1/2}H_\star M^{-1/2}) \leq \frac{1 + \theta}{1 - \theta}. \quad (46)$$

Proof. Since $\lambda_{\min}(H_\star) \geq \nu$,

$$\left\| H_\star^{-1/2}(H - H_\star)H_\star^{-1/2} \right\|_2 \leq \frac{\|H - H_\star\|_2}{\nu} \leq \theta. \quad (47)$$

Thus

$$(1 - \theta)H_\star \preceq H \preceq (1 + \theta)H_\star, \quad (48)$$

and hence

$$\frac{1}{1 + \theta}H \preceq H_\star \preceq \frac{1}{1 - \theta}H. \quad (49)$$

Writing $H = \alpha M$, with $\alpha = \det(H)^{1/n}$, gives

$$\frac{\alpha}{1 + \theta}M \preceq H_\star \preceq \frac{\alpha}{1 - \theta}M.$$

Premultiplying and postmultiplying by $M^{-1/2}$, all eigenvalues of $M^{-1/2}H_\star M^{-1/2}$ lie in

$$\left[\frac{\alpha}{1 + \theta}, \frac{\alpha}{1 - \theta} \right].$$

Therefore

$$\text{cond}(M^{-1/2}H_\star M^{-1/2}) \leq \frac{1 + \theta}{1 - \theta}.$$

□

Theorem 3.6 is not used as an additional assumption in the convergence proof. It explains the design: when the fully quadratic Hessian is relatively accurate for a locally positive definite true Hessian, the metric obtained from it nearly isotropizes the true local curvature.

3.5 Indefinite curvature and signed scaling

An interpolation Hessian need not be positive definite. The metric, however, must be SPD. Negative curvature should remain in the quadratic model used by the trust-region subproblem; it should not become a negative length scale in the region. The ideal nonsingular indefinite case can also be described exactly.

Proposition 3.7 (Signed isotropization by the absolute-curvature metric). *Let $H = V \text{diag}(\lambda_1, \dots, \lambda_n)V^\top$ be nonsingular and symmetric, and let*

$$|H| := V \text{diag}(|\lambda_1|, \dots, |\lambda_n|)V^\top, \quad M_{\text{abs}} := \frac{|H|}{\det(|H|)^{1/n}}. \quad (50)$$

Then

$$M_{\text{abs}}^{-1/2} H M_{\text{abs}}^{-1/2} = \det(|H|)^{1/n} V \text{diag}(\text{sign}(\lambda_1), \dots, \text{sign}(\lambda_n)) V^\top. \quad (51)$$

Proof. Let $\alpha = \det(|H|)^{1/n}$. Since $M_{\text{abs}}^{-1/2} = \alpha^{1/2} V \text{diag}(|\lambda_i|^{-1/2}) V^\top$, substitution gives (51). □

Thus the metric equalizes curvature magnitudes in induced variables, while the signs of the curvature directions are preserved in the model Hessian. An absolute-curvature shape changes only the length scale; it does not convexify the trust-region model. In practice, the fitted Hessian may be singular or nearly singular, so the construction uses a spectral floor.

Concretely, for an eigendecomposition

$$H_{x,k} = V \text{diag}(\lambda_1, \dots, \lambda_n) V^\top, \quad (52)$$

we form magnitudes

$$a_i = \max\{|\lambda_i|, \sigma\}, \quad i = 1, \dots, n, \quad (53)$$

where $\sigma > 0$ is a spectral floor. The resulting proxy

$$H_{\text{abs},k} := V \text{diag}(a_1, \dots, a_n) V^\top \quad (54)$$

is SPD. It should be interpreted as a curvature-shape proxy extracted from the fitted Hessian, not as a replacement for the signed Hessian in the subproblem.

3.6 A bounded spectral construction

The spectral rule used in the experiments converts $H_{\text{abs},k}$ into a bounded volume-normalized metric. Starting from (53), cap the ratio of largest to smallest entries by setting

$$\bar{a}_i = \max \left\{ a_i, \kappa_{\max}^{-1} \max_j a_j \right\}, \quad i = 1, \dots, n. \quad (55)$$

Then normalize the determinant:

$$\hat{a}_i = \frac{\bar{a}_i}{\left(\prod_{j=1}^n \bar{a}_j \right)^{1/n}}, \quad S_k = V \text{diag}(\hat{a}_1, \dots, \hat{a}_n) V^\top. \quad (56)$$

Thus $S_k \succ 0$, $\det(S_k) = 1$, and $\text{cond}(S_k) \leq \kappa_{\max}$. To avoid abrupt changes in induced coordinates, the final metric is chosen from

$$\mathcal{C}_k := \{ M \succ 0 : \det(M) = 1, \text{cond}(M) \leq \kappa_{\max}, \\ e^{-\delta_M} M_k \preceq M \preceq e^{\delta_M} M_k \}. \quad (57)$$

The final metric is obtained from S_k by taking a damped affine-invariant geodesic step from M_k toward S_k .

(S1) Relative eigendecomposition. Compute the symmetric relative matrix

$$C_k = M_k^{-1/2} S_k M_k^{-1/2} = P \text{diag}(\mu_1, \dots, \mu_n) P^\top, \quad P^\top P = I.$$

(S2) Geodesic damping. Set

$$\ell_i = \log \mu_i, \quad L_k = \max_{1 \leq i \leq n} |\ell_i|,$$

and define

$$\omega_k = \begin{cases} 1, & L_k = 0, \\ \min\{1, \delta_M / L_k\}, & L_k > 0. \end{cases}$$

(S3) Metric update. Return

$$M_{k+1} = M_k^{1/2} P \text{diag}(e^{\omega_k \ell_1}, \dots, e^{\omega_k \ell_n}) P^\top M_k^{1/2}.$$

Proposition 3.8 (Output of the spectral construction). *Suppose $M_k \succ 0$ with $\det(M_k) = 1$ and $\text{cond}(M_k) \leq \kappa_{\max}$, and let S_k be defined by (55)–(56). Then the metric M_{k+1} produced by steps (S1)–(S3) satisfies $M_{k+1} \in \mathcal{C}_k$.*

Proof. By (56), $S_k \succ 0$, $\det(S_k) = 1$, and $\text{cond}(S_k) \leq \kappa_{\max}$. Since $\det(M_k) = 1$, the relative matrix $C_k = M_k^{-1/2} S_k M_k^{-1/2}$ satisfies $\det(C_k) = 1$. Hence

$$\sum_{i=1}^n \ell_i = \log \det(C_k) = 0.$$

The update in (S3) has relative eigenvalues $e^{\omega_k \ell_i}$ with respect to M_k . Therefore

$$\det(M_{k+1}) = \det(M_k) \prod_{i=1}^n e^{\omega_k \ell_i} = 1$$

and, by the definition of ω_k ,

$$|\omega_k \ell_i| \leq \delta_M \quad \text{for all } i.$$

Thus

$$e^{-\delta_M} M_k \preceq M_{k+1} \preceq e^{\delta_M} M_k.$$

We now verify the condition-number cap. For this purpose, note that the update is the weighted affine-invariant geometric mean

$$M_{k+1} = M_k \#_{\omega_k} S_k.$$

For any $A, B \succ 0$ and $t \in [0, 1]$, monotonicity and homogeneity of the weighted geometric mean give

$$\lambda_{\max}(A \#_t B) \leq \lambda_{\max}(A)^{1-t} \lambda_{\max}(B)^t,$$

and, using $(A \#_t B)^{-1} = A^{-1} \#_t B^{-1}$,

$$\lambda_{\min}(A \#_t B) \geq \lambda_{\min}(A)^{1-t} \lambda_{\min}(B)^t.$$

Consequently,

$$\text{cond}(A \#_t B) \leq \text{cond}(A)^{1-t} \text{cond}(B)^t.$$

Applying this with $A = M_k$, $B = S_k$, and $t = \omega_k$, and using $\text{cond}(M_k) \leq \kappa_{\max}$ and $\text{cond}(S_k) \leq \kappa_{\max}$, yields

$$\text{cond}(M_{k+1}) \leq \text{cond}(M_k)^{1-\omega_k} \text{cond}(S_k)^{\omega_k} \leq \kappa_{\max}.$$

Therefore $M_{k+1} \in \mathcal{C}_k$. □

For convergence, only the properties summarized in Theorem 3.9 are needed. Theorem 3.8 shows that the construction above satisfies them.

Theorem 3.9 (Metric contract for the spectral construction). *Assume $M_0 \succ 0$, $\det(M_0) = 1$, and $\text{cond}(M_0) \leq \kappa_{\max}$. Suppose that the metric-selection routine returns $M_{k+1} \in \mathcal{C}_k$ for every k . Then*

$$\det(M_k) = 1, \quad \text{cond}(M_k) \leq \kappa_{\max}, \quad k = 0, 1, 2, \dots, \quad (58)$$

and

$$\kappa_{\max}^{-(n-1)/n} I \preceq M_k \preceq \kappa_{\max}^{(n-1)/n} I. \quad (59)$$

Moreover,

$$e^{-\delta_M/2} \|s\|_{M_k} \leq \|s\|_{M_{k+1}} \leq e^{\delta_M/2} \|s\|_{M_k} \quad \forall s \in \mathbb{R}^n. \quad (60)$$

Proof. The determinant and condition-number statements follow directly from $M_{k+1} \in \mathcal{C}_k$ and the initialization. Let $0 < \mu_1 \leq \dots \leq \mu_n$ be the eigenvalues of any $M \succ 0$ with $\det(M) = 1$ and $\text{cond}(M) \leq \kappa_{\max}$. Since $\mu_n/\mu_1 \leq \kappa_{\max}$ and $\prod_i \mu_i = 1$,

$$1 = \prod_{i=1}^n \mu_i \geq \mu_n \left(\frac{\mu_n}{\kappa_{\max}} \right)^{n-1} = \frac{\mu_n^n}{\kappa_{\max}^{n-1}}, \quad (61)$$

so $\mu_n \leq \kappa_{\max}^{(n-1)/n}$. Similarly,

$$1 = \prod_{i=1}^n \mu_i \leq \mu_1 (\kappa_{\max} \mu_1)^{n-1}, \quad (62)$$

so $\mu_1 \geq \kappa_{\max}^{-(n-1)/n}$. This proves (59). Finally, the Loewner inequalities in (57) imply

$$e^{-\delta_M} s^\top M_k s \leq s^\top M_{k+1} s \leq e^{\delta_M} s^\top M_k s. \quad (63)$$

Taking square roots gives (60). □

Corollary 3.10 (Nesting of consecutive metric balls). *Under the assumptions of Theorem 3.9, for every $x \in \mathbb{R}^n$ and $\Delta > 0$,*

$$\mathcal{B}_{M_k}(x, e^{-\delta_M/2}\Delta) \subseteq \mathcal{B}_{M_{k+1}}(x, \Delta) \subseteq \mathcal{B}_{M_k}(x, e^{\delta_M/2}\Delta). \quad (64)$$

Proof. The inclusions are exactly (60) written in terms of metric balls. \square

Theorems 3.9 and 3.10 provide the bridge from metric design to convergence. The construction can use curvature information when it is reliable, while the induced coordinate systems remain uniformly bounded and change gradually.

4 Convergence under the Metric Contract

We now verify that the abstract metric trust-region method is compatible with the standard fully quadratic convergence mechanism. The proof is stated in induced variables, where the trust region is Euclidean. The new ingredient is the uniform metric contract: it transfers smoothness, model accuracy, and stationarity between the original variables and the induced variables. Once this transfer is made, the decrease and radius-accounting arguments are the usual trust-region arguments.

4.1 Model accuracy in induced variables

The induced model \tilde{m}_k is fully quadratic for \tilde{f}_k on $\|y\| \leq \Delta_k$ if there exist constants $(\kappa_f^y, \kappa_g^y, \kappa_H^y)$ such that

$$|\tilde{f}_k(y) - \tilde{m}_k(y)| \leq \kappa_f^y \Delta_k^3, \quad (65)$$

$$\|\nabla \tilde{f}_k(y) - \nabla \tilde{m}_k(y)\| \leq \kappa_g^y \Delta_k^2, \quad (66)$$

$$\|\nabla^2 \tilde{f}_k(y) - B_{y,k}\|_2 \leq \kappa_H^y \Delta_k, \quad (67)$$

for all $\|y\| \leq \Delta_k$.

Assumption 4.1 (Regularity and model accuracy). *There is a region $\mathcal{R} \subset \mathbb{R}^n$ containing all induced trust-region balls*

$$\{x_k + M_k^{-1/2}y : \|y\| \leq \Delta_k\}, \quad k = 0, 1, \dots,$$

such that f is bounded below by f_\star on \mathcal{R} , has an L_2 -Lipschitz Hessian on \mathcal{R} , and satisfies

$$\sup_{x \in \mathcal{R}} \|\nabla^2 f(x)\|_2 \leq H_f < \infty.$$

Theorem 2.5 holds. The interpolation sets are uniformly Λ -poised in the current metric ball, so that the induced models are fully quadratic with constants independent of k .

The stationarity measure used by the algorithm is the induced model-gradient norm $\chi_k = \|g_{y,k}\|$. The corresponding true stationarity measure is

$$\chi_k^{\text{true}} = \|\nabla f(x_k)\|_{M_k^{-1}} = \|M_k^{-1/2} \nabla f(x_k)\|. \quad (68)$$

Indeed, $\nabla \tilde{f}_k(0) = M_k^{-1/2} \nabla f(x_k)$, so $\chi_k^{\text{true}} = \|\nabla \tilde{f}_k(0)\|$.

Proposition 4.2 (Uniform fully quadratic constants). *Assume f has an L_2 -Lipschitz Hessian on the sampled region and that Theorem 2.5 holds. Then each induced function $\tilde{f}_k(y) = f(x_k + M_k^{-1/2}y)$ has Lipschitz Hessian constant at most $L_2 m_{\min}^{-3/2}$. Consequently, if the interpolation sets are uniformly Λ -poised in the induced balls, the fully quadratic constants in (65)–(67) can be chosen independently of k .*

Proof. For any y, z in the induced ball, set $\xi_y = x_k + M_k^{-1/2}y$ and $\xi_z = x_k + M_k^{-1/2}z$. Then

$$\begin{aligned} \left\| \nabla^2 \tilde{f}_k(y) - \nabla^2 \tilde{f}_k(z) \right\|_2 &= \left\| M_k^{-1/2} (\nabla^2 f(\xi_y) - \nabla^2 f(\xi_z)) M_k^{-1/2} \right\|_2 \\ &\leq \left\| M_k^{-1/2} \right\|_2^2 L_2 \|\xi_y - \xi_z\| \\ &\leq L_2 \left\| M_k^{-1/2} \right\|_2^3 \|y - z\| \leq L_2 m_{\min}^{-3/2} \|y - z\|. \end{aligned} \quad (69)$$

The standard poisedness-to-fully-quadratic result for full quadratic interpolation then gives uniform constants depending only on n, Λ , and the induced Lipschitz constant. \square

Assumption 4.3 (Criticality safeguard). *There exists $\mu_{\text{crit}} > 0$ with $\kappa_g^y \mu_{\text{crit}}^2 \leq 1/2$ such that, whenever $\chi_k \leq 1$, the algorithm enforces*

$$\Delta_k \leq \mu_{\text{crit}} \chi_k. \quad (70)$$

Assumption 4.4 (Sufficient decrease and radius update). *There exist $c_{\text{dec}} > 0$ and a uniform upper bound \bar{h} on $\|B_{y,k}\|_2$ such that the trial step satisfies*

$$\text{pred}_k \geq c_{\text{dec}} \min \left\{ \frac{\chi_k^2}{\bar{h}_+}, \Delta_k \chi_k \right\}, \quad \bar{h}_+ := \max\{\bar{h}, 1\}. \quad (71)$$

The trust-region update uses constants $0 < \eta_1 \leq \eta_2 < 1$ and $0 < \gamma_{\text{dec}} < 1 < \gamma_{\text{inc}}$, and a maximum radius Δ_{max} . Rejected iterations shrink the radius by γ_{dec} ; very successful iterations with $\rho_k \geq \eta_2$ increase the radius by at least γ_{inc} , unless the maximum radius is active; all radii remain bounded by Δ_{max} .

The uniform bound \bar{h} is consistent with Theorem 4.1: for all $\|y\| \leq \Delta_k$,

$$\|\nabla^2 \tilde{f}_k(y)\|_2 \leq \|M_k^{-1/2}\|_2^2 H_f \leq m_{\min}^{-1} H_f.$$

Together with the fully quadratic Hessian error bound, this gives for example

$$\|B_{y,k}\|_2 \leq m_{\min}^{-1} H_f + \kappa_H^y \Delta_{\text{max}},$$

so a finite uniform \bar{h} may be chosen.

4.2 Acceptance at small radii

The complexity proof uses model accuracy in two places: to compare model and true stationarity, and to compare actual and predicted reduction.

Lemma 4.5 (Stationarity transfer). *Under Theorem 4.1,*

$$\left| \chi_k^{\text{true}} - \chi_k \right| \leq \kappa_g^y \Delta_k^2. \quad (72)$$

If additionally Theorem 4.3 holds and $\chi_k \leq 1$, then

$$\chi_k \geq \frac{2}{3} \chi_k^{\text{true}}. \quad (73)$$

Proof. The gradient bound (66) at $y = 0$ gives

$$\left\| M_k^{-1/2} \nabla f(x_k) - g_{y,k} \right\| = \left\| \nabla \tilde{f}_k(0) - \nabla \tilde{m}_k(0) \right\| \leq \kappa_g^y \Delta_k^2. \quad (74)$$

The reverse triangle inequality gives (72). If $\chi_k \leq 1$, then by the criticality safeguard,

$$\kappa_g^y \Delta_k^2 \leq \kappa_g^y \mu_{\text{crit}}^2 \chi_k^2 \leq \frac{1}{2} \chi_k^2 \leq \frac{1}{2} \chi_k. \quad (75)$$

Therefore $\chi_k^{\text{true}} \leq \chi_k + \frac{1}{2} \chi_k = \frac{3}{2} \chi_k$, which is (73). \square

Lemma 4.6 (Actual–predicted reduction error). *Under Theorem 4.1,*

$$|\text{ared}_k - \text{pred}_k| \leq 2\kappa_f^y \Delta_k^3. \quad (76)$$

Proof. With $s_k = T_k^{-1}y_k$, we have $\tilde{f}_k(0) = f(x_k)$ and $\tilde{f}_k(y_k) = f(x_k + s_k)$. Hence

$$\text{ared}_k - \text{pred}_k = (\tilde{m}_k(y_k) - \tilde{f}_k(y_k)) - (\tilde{m}_k(0) - \tilde{f}_k(0)). \quad (77)$$

Each term is bounded in absolute value by $\kappa_f^y \Delta_k^3$ from (65). \square

Lemma 4.7 (Acceptance below the critical radius). *Assume Theorems 4.1, 4.3, and 4.4. Fix $\varepsilon \in (0, 1)$ and suppose $\chi_k^{\text{true}} > \varepsilon$. Define*

$$\Delta_\varepsilon^{\text{vs}} := \min \left\{ \left(\frac{(1 - \eta_2)c_{\text{dec}}\varepsilon}{3\kappa_f^y} \right)^{1/2}, \frac{2\varepsilon}{3\bar{h}_+}, \frac{\Delta_{\text{max}}}{\gamma_{\text{inc}}} \right\}. \quad (78)$$

If $\Delta_k \leq \Delta_\varepsilon^{\text{vs}}$, then the iteration is very successful: $\rho_k \geq \eta_2$, and the radius is increased by at least γ_{inc} .

Proof. If $\chi_k \leq 1$, then Theorem 4.5 gives $\chi_k \geq (2/3)\chi_k^{\text{true}} > 2\varepsilon/3$. If $\chi_k > 1$, the same lower bound holds because $\varepsilon < 1$. Thus $\chi_k \geq 2\varepsilon/3$ in all cases. Since $\Delta_k \leq 2\varepsilon/(3\bar{h}_+) \leq \chi_k/\bar{h}_+$, Theorem 4.4 gives

$$\text{pred}_k \geq c_{\text{dec}}\Delta_k\chi_k \geq \frac{2}{3}c_{\text{dec}}\varepsilon\Delta_k. \quad (79)$$

Together with Theorem 4.6,

$$|\rho_k - 1| \leq \frac{2\kappa_f^y \Delta_k^3}{\text{pred}_k} \leq \frac{3\kappa_f^y \Delta_k^2}{c_{\text{dec}}\varepsilon} \leq 1 - \eta_2. \quad (80)$$

Hence $\rho_k \geq \eta_2$. The definition of $\Delta_\varepsilon^{\text{vs}}$ also ensures $\Delta_k \leq \Delta_{\text{max}}/\gamma_{\text{inc}}$, so the update increases the radius by at least γ_{inc} . \square

4.3 Evaluation complexity

The final ingredient is the standard radius-accounting argument: below the threshold $\Delta_\varepsilon^{\text{vs}}$, iterations are very successful and push the radius upward, whereas large successful iterations decrease the objective by a fixed multiple of ε^2 . The following theorem states the resulting bound for an arbitrary prefix of iterations on which the target stationarity has not yet been reached.

Theorem 4.8 (First-order evaluation complexity). *Assume Theorems 4.1, 4.3, and 4.4. Let $\varepsilon \in (0, 1)$, and suppose $\chi_k^{\text{true}} > \varepsilon$ for $k = 0, 1, \dots, N - 1$. Then*

$$N = \mathcal{O}(\varepsilon^{-2}). \quad (81)$$

Consequently the first hitting time $N_\varepsilon := \min\{k : \chi_k^{\text{true}} \leq \varepsilon\}$ exists and satisfies the same order bound. If each geometry-repair event uses at most $C_{\text{geom}}q_n$ new function evaluations for a constant independent of ε , then the evaluation complexity is

$$\mathcal{O}(q_n\varepsilon^{-2}) = \mathcal{O}(n^2\varepsilon^{-2}). \quad (82)$$

Proof. For every $k < N$, the proof of Theorem 4.7 shows that $\chi_k \geq 2\varepsilon/3$. Consider a successful iteration with $\Delta_k \geq \Delta_\varepsilon^{\text{vs}}$. By the sufficient decrease condition,

$$f(x_k) - f(x_{k+1}) \geq \eta_1 c_{\text{dec}} \min \left\{ \frac{4\varepsilon^2}{9\bar{h}_+}, \frac{2}{3}\varepsilon\Delta_\varepsilon^{\text{vs}} \right\} \geq c_s\varepsilon^2, \quad (83)$$

where $c_s > 0$ is independent of ε . The last inequality uses $\Delta_\varepsilon^{\text{vs}} \geq c_\Delta \varepsilon$ for a constant $c_\Delta > 0$, which follows from $0 < \varepsilon < 1$ because every term in $\Delta_\varepsilon^{\text{vs}}$ is bounded below by a positive constant times ε . Since f is bounded below, the number of such large-radius successful iterations is $\mathcal{O}(\varepsilon^{-2})$.

By Theorem 4.7, every iteration with $\Delta_k \leq \Delta_\varepsilon^{\text{vs}}$ is very successful and increases the radius by at least γ_{inc} . Rejected iterations shrink the radius by γ_{dec} , and all radii remain bounded above by Δ_{max} . A logarithmic radius-accounting argument then shows that the number of unsuccessful iterations and small-radius successful iterations is bounded by a constant multiple of the number of large-radius successful iterations plus $1 + |\log(\Delta_0/\Delta_\varepsilon^{\text{vs}})|$. Since this logarithmic term is $\mathcal{O}(\log(1/\varepsilon)) = \mathcal{O}(\varepsilon^{-2})$ for $0 < \varepsilon < 1$, we obtain $N = \mathcal{O}(\varepsilon^{-2})$.

Each main iteration uses one trial evaluation. Maintaining a fully quadratic model may require geometry repair, and by assumption each repair event costs at most $C_{\text{geom}}q_n$ new evaluations. Hence the total evaluation count is $\mathcal{O}(q_n N) = \mathcal{O}(n^2 \varepsilon^{-2})$. Since no prefix longer than this bound can satisfy $\chi_k^{\text{true}} > \varepsilon$ throughout, N_ε exists and obeys the same bound. \square

Corollary 4.9 (Global first-order convergence). *Under the assumptions of Theorem 4.8,*

$$\liminf_{k \rightarrow \infty} \chi_k^{\text{true}} = 0. \quad (84)$$

Proof. Fix any $\varepsilon \in (0, 1)$. Theorem 4.8 implies that an iteration with $\chi_k^{\text{true}} \leq \varepsilon$ occurs after finitely many iterations. Applying this to a sequence $\varepsilon_j \downarrow 0$ gives a subsequence along which $\chi_k^{\text{true}} \rightarrow 0$. \square

Remark 4.10 (Dependence of the implicit constant on problem data). The constant hidden in the $\mathcal{O}(\cdot)$ notation of Theorem 4.8 depends on $f(x_0) - f_{\text{low}}$ (the initial optimality gap), \bar{h}_+ (the uniform upper bound on Hessian norms), κ_{max} (the metric condition-number cap), $\eta_1, \gamma_{\text{dec}}, \gamma_{\text{inc}}$ (the trust-region management parameters), and Δ_{max} . In particular, it does *not* depend on the specific sequence of metrics $\{M_k\}$, because the spectral contract (Theorem 3.9) confines all metrics to the same compact set. The dependence on κ_{max} enters through the Cauchy decrease constant c_{dec} in Theorem 2.3 and vanishes when the metric is the identity, recovering the standard trust-region bound.

5 Numerical Experiments

The experiments examine the metric construction from three complementary angles. The Moré–Wild benchmark gives a standard comparison with established DFO solvers. A controlled anisotropy study tests the central mechanism more directly by rotating and rescaling benchmark problems. Two-dimensional trajectories then show how the computed ellipsoids behave along individual runs. Together these experiments are meant to illustrate the cost–accuracy trade-off of building a full quadratic curvature metric, not to replace the deterministic convergence guarantees proved above.

5.1 Experimental protocol

All experiments use the Moré–Wild budget convention: one simplex gradient corresponds to $n + 1$ function evaluations [9]. A run is declared solved at tolerance τ if it reaches the Moré–Wild threshold

$$f(x) - f_\star \leq \tau(f(x_0) - f_\star) \quad (85)$$

within the evaluation budget, with the implementation using the standard f_\star -scaled absolute fallback when the initial gap is nonpositive. Unless stated otherwise, the budget is $500(n + 1)$ evaluations. The reported final relative error is

$$\frac{|f(x) - f_\star|}{\max\{|f_\star|, |f(x_0) - f_\star|, 1\}}.$$

Table 2: Solve rates (%) on the Moré–Wild benchmark over 37 instances and five seeds.

Solver	$\tau = 10^{-1}$	$\tau = 10^{-3}$	$\tau = 10^{-5}$	$\tau = 10^{-7}$
MATRO	86.5	83.8	83.8	75.7
NEWUOA	64.9	59.5	51.4	48.6
UOBYQA	62.2	62.2	51.4	48.6
Nelder–Mead	78.4	78.4	78.4	64.9
CMA-ES	86.5	86.5	76.2	66.5

The parallel experiment harness uses per-task wall-clock cutoffs to avoid hung runs: 300 seconds in the standard Moré–Wild benchmark and 60 seconds in the controlled-anisotropy study. A run that exhausts either the evaluation budget or the applicable wall-clock cutoff before reaching tolerance τ is recorded as a failure at τ . These conventions apply uniformly to all solvers. MATRO uses the spectral metric construction described in Section 3.6, with

$$\begin{aligned} \eta_1 = 0.1, \quad \eta_2 = 0.5, \quad \gamma_{\text{dec}} = 0.5, \quad \gamma_{\text{inc}} = 2.5, \\ \sigma = 10^{-8}, \quad \kappa_{\text{max}} = 10^6, \quad \delta_M = 1.0. \end{aligned} \tag{86}$$

All solvers use the same starting points. Random seeds are shared across randomized transformations and stochastic solvers; deterministic solvers are run on the same transformed instances.

5.2 Standard benchmark behavior

The first experiment uses the Moré–Wild benchmark collection: 22 problem families, 37 instances, and dimensions $n \in \{2, \dots, 12\}$. We compare MATRO with four baselines: NEWUOA, UOBYQA, Nelder–Mead [10], and CMA-ES [7]. UOBYQA is the closest spherical full-quadratic baseline because it uses the same order of interpolation points as MATRO. NEWUOA is the lower-cost minimum-change baseline, using only $2n + 1$ interpolation points. Nelder–Mead and CMA-ES are included as classical non-trust-region baselines.

Table 2 shows that MATRO achieves the highest solve rates at moderate-to-tight tolerances. At $\tau = 10^{-1}$, MATRO and CMA-ES both reach 86.5%, ahead of the classical trust-region solvers. At $\tau = 10^{-5}$, MATRO leads with 83.8%, followed by Nelder–Mead (78.4%) and CMA-ES (76.2%). At $\tau = 10^{-7}$, MATRO solves 75.7% of the runs, compared with 66.5% for CMA-ES and 64.9% for Nelder–Mead. NEWUOA and UOBYQA show substantial timeout rates on the larger instances, so their solve rates should be interpreted together with the wall-clock cutoff. This pattern is consistent with the intended role of the metric: curvature information becomes more informative once the interpolation model is accurate enough to capture the local geometry.

The data profiles in Figure 2 and the Dolan–Moré performance profiles in Figure 3 [6] give the same trend at the profile level. At small budgets, CMA-ES and Nelder–Mead begin moving without first constructing a full quadratic interpolation model. As the budget and required accuracy increase, the full quadratic metric has more opportunity to use curvature information, and MATRO attains a larger solved fraction. The performance profiles also show that the relative ranking is problem dependent, as expected for a method whose advantage depends on the presence of stable local anisotropy.

The per-problem convergence curves support the aggregate profiles. On classical problems such as Rosenbrock and Powell, MATRO converges comparably or faster than the spherical baselines. Its advantage is most visible on instances where NEWUOA and UOBYQA exhaust the budget before reaching moderate accuracy, such as Watson ($n = 9$), Chebyquad ($n = 9$), Osborne 1, and Osborne 2.

Figure 4 illustrates these regimes; the full set of per-problem curves is available with the plotting scripts in the repository.

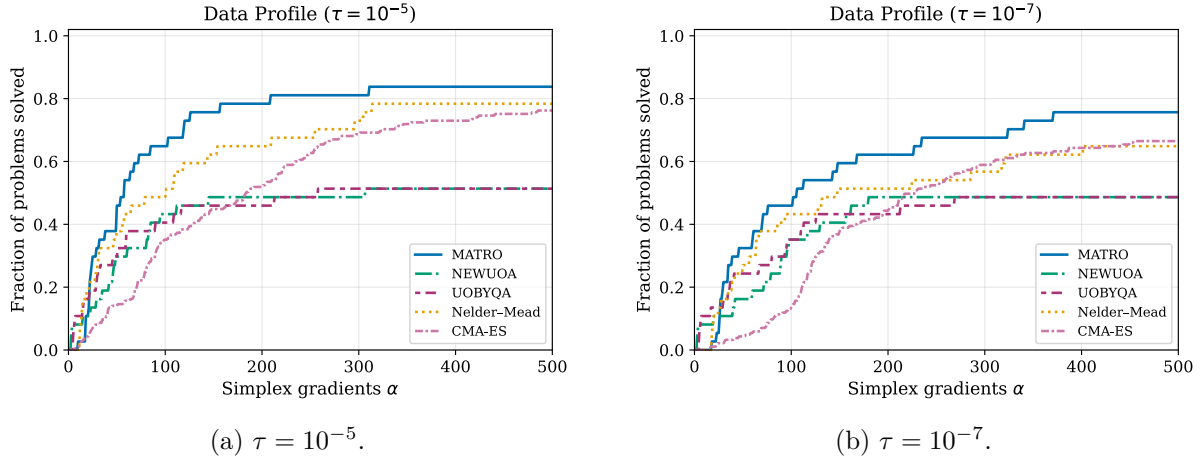


Figure 2: Data profiles on the Moré–Wild benchmark.

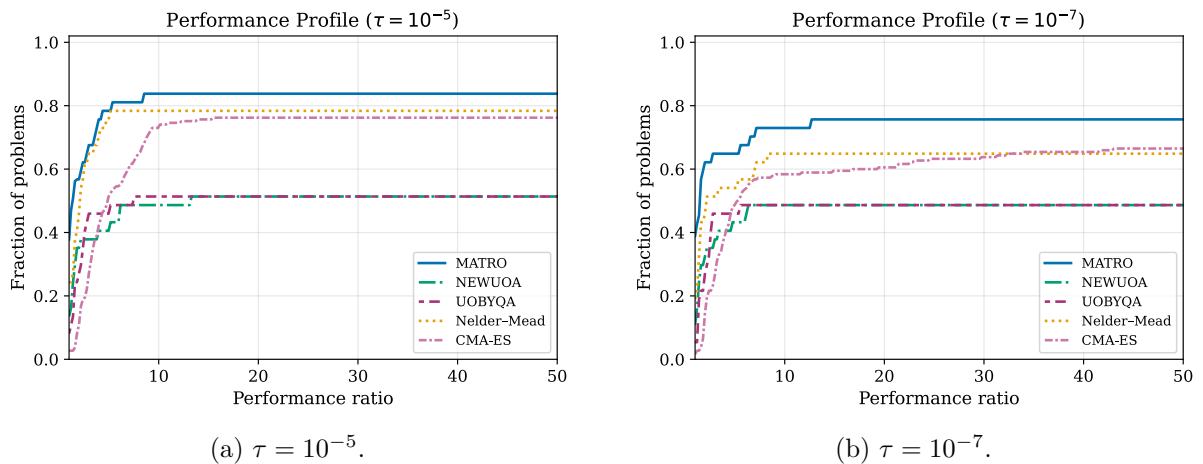


Figure 3: Dolan–Moré performance profiles on the Moré–Wild benchmark.

5.3 Response to controlled anisotropy

The second experiment isolates the effect of anisotropy more directly. We transform each base problem by

$$g(x) = f(Ax + b), \quad A = Q \operatorname{diag}(\sigma_1, \dots, \sigma_n) Q^\top, \quad \operatorname{cond}(A) = \kappa, \quad (87)$$

where Q is a random orthogonal matrix and the singular values σ_i are geometrically spaced between 1 and κ . At $\kappa = 1$, all σ_i are equal and the transformation is orthogonal up to scaling. The base problems are Rosenbrock ($n = 5$), Powell ($n = 4$), Ellipsoid ($n = 5$), Wood ($n = 4$), and Chebyquad ($n = 6$), each with $\kappa \in \{1, 10, 20, 30, \dots, 100\}$. For each (problem, κ) setting, five random rotations and five solver seeds give 25 independent runs. We compare MATRO with NEWUOA.

The median NFEV values are computed over solved runs only and should therefore be interpreted together with the solve-rate table.

Figure 5 and Table 3 show how increasing anisotropy changes the relative behavior of the two solvers. At $\kappa = 1$, both solvers succeed on most problems; NEWUOA is faster on the well-conditioned Ellipsoid instance because it uses a smaller interpolation set. As κ grows, NEWUOA’s solve rate drops sharply on Chebyquad (reaching 0% at $\kappa \geq 40$), Rosenbrock (0% at $\kappa \geq 30$), and Powell (below 50% at $\kappa \geq 40$), whereas MATRO maintains 100% on all five problems across the entire range. On Ellipsoid, NEWUOA retains a partial solve rate but its median NFEV grows more rapidly than MATRO’s. The MATRO NFEV curves are nearly flat:

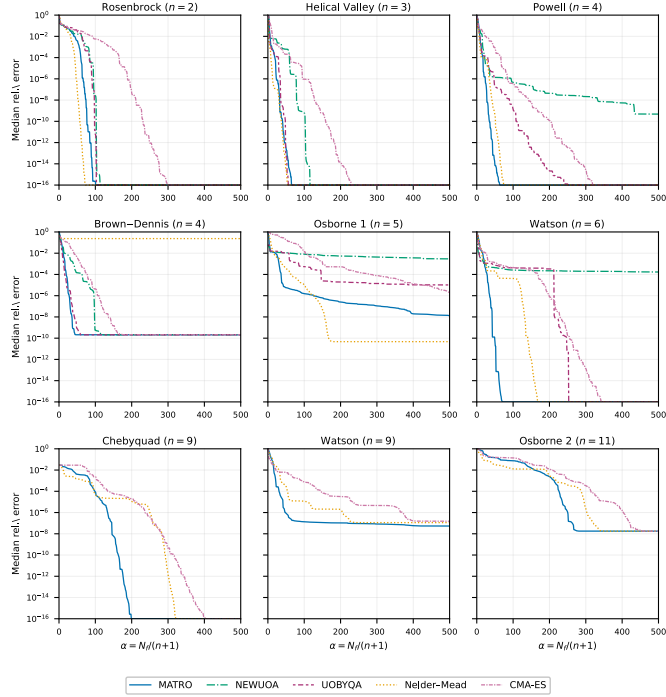


Figure 4: Per-problem convergence on nine representative Moré–Wild instances (median over five seeds).

Table 3: Solve rates (%) on the controlled-anisotropy study at $\tau = 10^{-3}$, over 25 runs per setting. Here M denotes MATRO and N denotes NEWUOA; a zero entry means that no run was solved.

κ	Chebyquad		Ellipsoid		Powell		Rosenbrock		Wood	
	M	N	M	N	M	N	M	N	M	N
1	100	100	100	100	100	100	100	40	100	100
10	100	100	100	92	100	100	100	60	100	100
20	100	60	100	96	100	100	100	60	100	100
30	100	20	100	88	100	80	100	0	100	100
40	100	0	100	88	100	40	100	0	100	100
50	100	0	100	68	100	40	100	0	100	100
60	100	0	100	80	100	60	100	0	100	100
70	100	0	100	76	100	40	100	0	100	100
80	100	0	100	68	100	60	100	0	100	100
90	100	0	100	64	100	20	100	0	100	100
100	100	0	100	72	100	40	100	0	100	80

the metric absorbs the conditioning increase into the trust-region shape, so that the subproblem in induced variables sees a much smaller effective condition number. The tighter-tolerance tables and raw data are available in the accompanying repository.

5.4 Trajectory-level geometry

The third experiment visualizes the mechanism on two-dimensional problems. The goal is qualitative: the plots show how the metric changes the trust-region shape along a trajectory and how this geometry relates to the observed error curves.

Figure 6 illustrates the mechanism at the trajectory level. The JSON data used to render these plots are included in the accompanying repository.

Median NFEV vs. condition number ($\tau = 10^{-3}$)

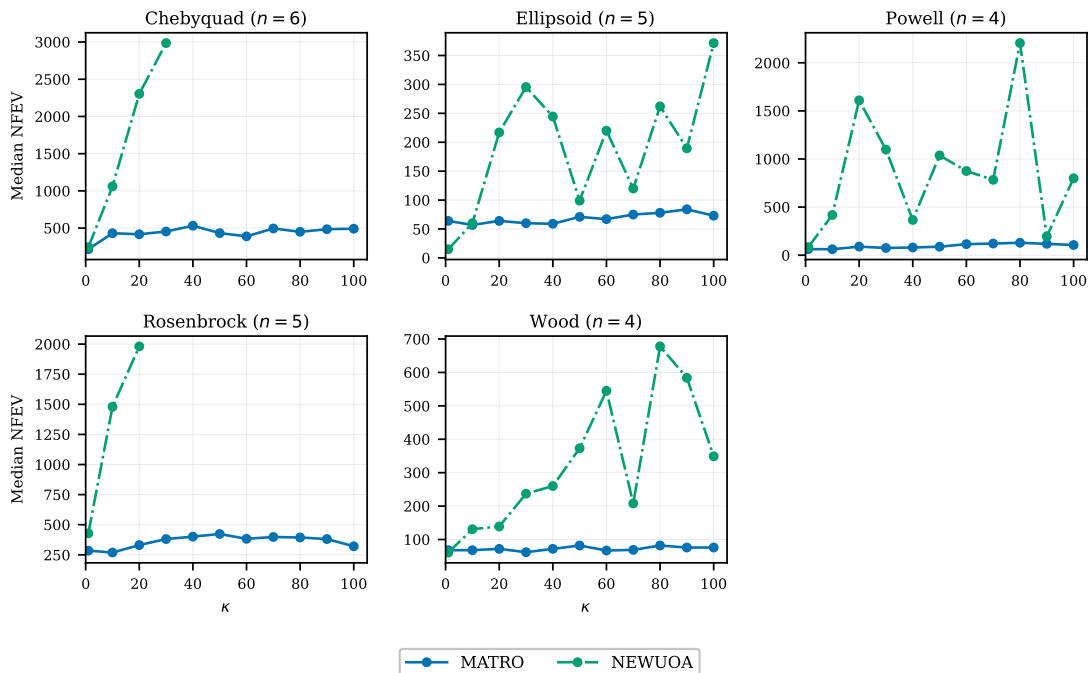


Figure 5: Median NFEV versus condition number κ at $\tau = 10^{-3}$. Each panel shows one base problem; medians are taken over solved runs among 25 independent instances per κ . A missing marker indicates that no run in that group was solved.

5.5 Cost and observed limitations

The cost of the curvature metric is concentrated in dense linear algebra. Each MATRO iteration performs an $\mathcal{O}(n^3)$ eigendecomposition of $H_{x,k}$ and stores an $\mathcal{O}(n^2)$ metric matrix. This cost is modest when function evaluations dominate, but it can be visible on analytic benchmark functions where evaluations are cheap. The initialization cost is also larger than for NEWUOA: MATRO requires $q_n = (n + 1)(n + 2)/2$ interpolation points before the first full quadratic model is available.

The observed limitations are consistent with the role assigned to the metric. If the interpolation Hessian is inaccurate, the metric may align with numerical or sampling artifacts. If many eigenvalues are controlled by the spectral floor or cap, the metric may underuse genuine curvature. In strongly nonconvex regions, a positive definite magnitude-based shape may not be the best search geometry. These cases mark the boundary between reliable local curvature information and curvature information that is not yet accurate enough to define the trust-region shape.

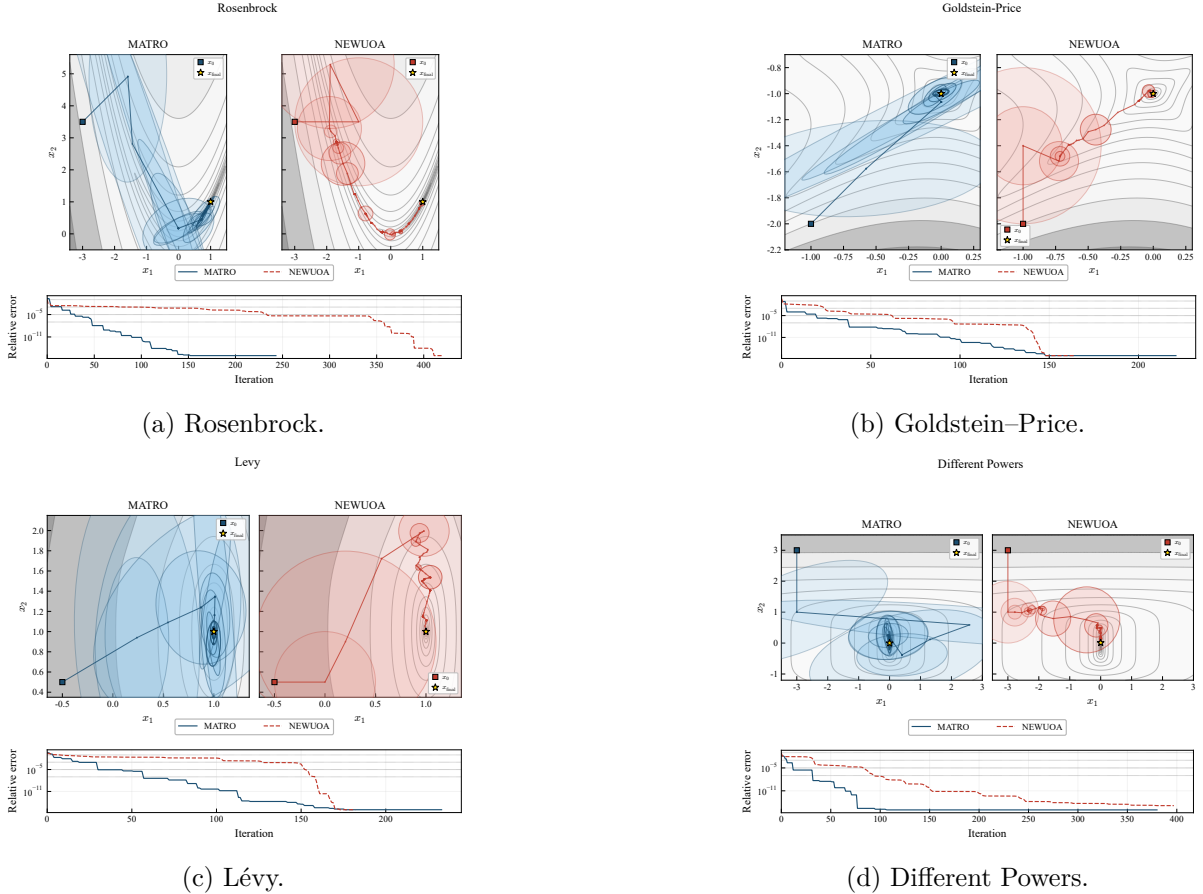


Figure 6: Two-dimensional trajectories. MATRO uses ellipsoidal regions and NEWUOA uses circular regions. The examples show valley alignment, metric rotation, a nearly isotropic case, and changing curvature ratios.

6 Conclusion

This paper developed MATRO, a fully quadratic derivative-free trust-region method in which the trust region is an ellipsoid and the metric is selected from interpolation curvature. The analysis first treats the metric abstractly: after the induced-coordinate map, the ellipsoidal subproblem is an ordinary Euclidean trust-region subproblem, and classical poisedness and fully quadratic theory apply in those coordinates. This shows that changing the trust-region geometry need not change the deterministic trust-region globalization mechanism, provided the metrics satisfy a uniform spectral contract.

The metric-selection analysis then explains why a Hessian-derived metric is an appropriate choice. For positive definite quadratics, the determinant-normalized curvature metric is the unique volume-normalized metric that makes the induced Hessian isotropic. The associated metric trust-region step is a truncated Newton step, and exact recovery occurs once the Newton step is feasible. For indefinite fitted Hessians, the absolute-curvature metric balances the magnitudes of curvature directions while preserving their signs in the induced model. Fully quadratic Hessian accuracy gives a corresponding bound on the induced conditioning of the true local Hessian.

Under the metric contract and the standard fully quadratic assumptions, the method retains the usual first-order evaluation-complexity order $\mathcal{O}(n^2\varepsilon^{-2})$ for full quadratic interpolation. The numerical experiments support the intended geometry-dependent interpretation. The ellipsoidal region is most helpful when the interpolation Hessian captures a stable anisotropic shape, especially in rotated or poorly scaled local geometries. Its cost is most visible at loose tolerances

and in problems where function evaluations are cheap relative to dense linear algebra.

Several directions remain open. The most immediate is to reduce the cost of metric selection through diagonal, block-diagonal, low-rank, or lazy-update variants. A second is to design more robust curvature-shape proxies in noisy or strongly nonconvex regimes. A third is to combine metric selection with underdetermined or regression-based quadratic models, so that the benefits of ellipsoidal trust regions are not tied to the full $\mathcal{O}(n^2)$ interpolation cost.

Source code and scripts for the experiments are available at <https://github.com/huwei0121/DFOETR>.

Reproducibility. The complete raw data, plotting scripts, per-problem convergence curves, the controlled-anisotropy tables at the tighter tolerance, and the two-dimensional trajectory JSON files are included in the accompanying repository. The main algorithmic parameters used to generate the figures are those listed in (86); the full implementation configuration is recorded with the experiment outputs.

References

- [1] C. Audet and J. E. Dennis, Jr., Mesh adaptive direct search algorithms for constrained optimization, *SIAM J. Optim.*, 17 (2006), pp. 188–217.
- [2] A. R. Conn, N. I. M. Gould, and P. L. Toint, *Trust-Region Methods*, MPS–SIAM Ser. Optim., SIAM, Philadelphia, PA, 2000.
- [3] A. R. Conn, K. Scheinberg, and L. N. Vicente, Geometry of interpolation sets in derivative free optimization, *Math. Program.*, 111 (2008), pp. 141–172.
- [4] A. R. Conn, K. Scheinberg, and L. N. Vicente, Geometry of sample sets in derivative-free optimization: polynomial regression and underdetermined interpolation, *IMA J. Numer. Anal.*, 28 (2008), pp. 721–748.
- [5] A. R. Conn, K. Scheinberg, and L. N. Vicente, *Introduction to Derivative-Free Optimization*, MPS–SIAM Ser. Optim., SIAM, Philadelphia, PA, 2009.
- [6] E. D. Dolan and J. J. Moré, Benchmarking optimization software with performance profiles, *Math. Program.*, 91 (2002), pp. 201–213.
- [7] N. Hansen, S. D. Müller, and P. Koumoutsakos, Reducing the time complexity of the derandomized evolution strategy with covariance matrix adaptation (CMA-ES), *Evol. Comput.*, 11 (2003), pp. 1–18.
- [8] J. Larson, M. Menickelly, and S. M. Wild, Derivative-free optimization methods, *Acta Numer.*, 28 (2019), pp. 287–404.
- [9] J. J. Moré and S. M. Wild, Benchmarking derivative-free optimization algorithms, *SIAM J. Optim.*, 20 (2009), pp. 172–191.
- [10] J. A. Nelder and R. Mead, A simplex method for function minimization, *Comput. J.*, 7 (1965), pp. 308–313.
- [11] M. J. D. Powell, UOBYQA: Unconstrained optimization by quadratic approximation, *Math. Program.*, 92 (2002), pp. 555–582.
- [12] M. J. D. Powell, The NEWUOA software for unconstrained optimization without derivatives, in *Large-Scale Nonlinear Optimization*, G. Di Pillo and M. Roma, eds., Nonconvex Optim. Appl. 83, Springer, New York, 2006, pp. 255–297.

- [13] M. J. D. Powell, The BOBYQA algorithm for bound constrained optimization without derivatives, Tech. Rep. DAMTP 2009/NA06, Department of Applied Mathematics and Theoretical Physics, University of Cambridge, Cambridge, UK, 2009.
- [14] S. M. Wild and C. A. Shoemaker, Global convergence of radial basis function trust-region derivative-free algorithms, *SIAM J. Optim.*, 21 (2011), pp. 761–781.
- [15] P. Xie and Y. Yuan, A derivative-free method using a new underdetermined quadratic interpolation model, *SIAM J. Optim.*, 35 (2025), pp. 1110–1133.
- [16] P. Xie and Y. Yuan, Least H^2 -norm updating of quadratic interpolation models for derivative-free trust-region algorithms, *IMA J. Numer. Anal.*, 46 (2026), pp. 21–50.
- [17] L. Li, Y. Zhou, P. Xie, and H. Li, “A spectral Levenberg–Marquardt–deflation method for multiple solutions of semilinear elliptic systems,” *Journal of Computational and Applied Mathematics*, vol. 475, article 116998, 2025.
- [18] Y. Ye, L. Li, P. Xie, and H. Yu, “An improved adaptive orthogonal basis deflation method for multiple solutions with applications to nonlinear elliptic equations in varying domains,” *Journal of Computational Mathematics*, vol. 44, no. 3, pp. 794–818, 2025.
- [19] P. Xie and Y.-x. Yuan, “A derivative-free optimization algorithm combining line-search and trust-region techniques,” *Chinese Annals of Mathematics, Series B*, vol. 44, no. 5, pp. 693–708, 2023.
- [20] P. Xie and S. M. Wild, ReMU: regional minimal updating for model-based derivative-free optimization, *Optim. Methods Softw.*, published online, 2026.
- [21] P. Xie and Y. Yuan, Derivative-free optimization with transformed objective functions and the algorithm based on the least Frobenius norm updating quadratic model, *J. Oper. Res. Soc. China*, 13 (2025), pp. 327–363.
- [22] P. Xie and Y. Yuan, A new two-dimensional model-based subspace method for large-scale unconstrained derivative-free optimization: 2D-MoSub, *Optim. Methods Softw.*, 41 (2026), pp. 118–150.
- [23] Z. Zhang, PRIMA: Reference implementation for Powell’s methods with modernization and amelioration, preprint, arXiv:2307.12962, 2023.